

Flame Acceleration in Channels with Obstacles in the Deflagration-to-Detonation Transition

Damir Valiev¹, Vitaly Bychkov¹, Vyacheslav Akkerman², Chung K. Law², and Lars-Erik Eriksson³

¹*Department of Physics, Umeå University, 901 87 Umeå, Sweden*

²*Department of Mechanical and Aerospace Engineering,
Princeton University, Princeton, NJ 08544-5263, USA*

³*Department of Applied Mechanics, Chalmers University of Technology, 412 96 Gothenburg, Sweden*

Abstract

It was demonstrated recently in Bychkov et al., Phys. Rev. Lett. 101 (2008) 164501, that the physical mechanism of flame acceleration in channels with obstacles is qualitatively different from the classical Shelkin mechanism. The new mechanism is much stronger, and is independent of the Reynolds number. The present study provides details of the theory and numerical modeling of the flame acceleration. It is shown theoretically and computationally that flame acceleration progresses noticeably faster in the axisymmetric cylindrical geometry as compared to the planar one, and that the acceleration rate reduces with increasing initial Mach number and thereby the gas compressibility. Furthermore, the velocity of the accelerating flame saturates to a constant value that is supersonic with respect to the wall. The saturation state can be correlated to the Chapman-Jouguet deflagration as well as the fast flames observed in experiments. The possibility of transition from deflagration to detonation in the obstructed channels is demonstrated.

1. INTRODUCTION

In the process of deflagration-to-detonation transition (DDT) in tubes with a closed end, a slow premixed flame accelerates spontaneously from the closed end and triggers detonation [1–13]. A qualitative explanation of the process was first proposed by Shelkin, Ref. [1]. According to this scenario, the burned gas expands and drives a flow in the fuel mixture. The flow becomes nonuniform because of the no-slip boundary condition at the wall which, together with turbulence, distorts the flame front, increases the burning rate, and leads to the acceleration. An accelerating flame front pushes compression waves that continuously heat the fuel mixture ahead of it until an explosion is triggered that eventually develops into a detonation.

While the Shelkin mechanism relies prominently on the action of turbulence, it was recently shown theoretically that flame acceleration is possible even in its absence, in tubes with smooth adiabatic wall [14, 15]. This theory has been validated by extensive numerical simulations in Refs. [14, 15] and supported by experiments in smooth micro-tubes [16]. The theory and modeling further demonstrate that laminar flame acceleration becomes quite weak in wide tubes with increasing Reynolds number of the flow, and as such loss to the wall may actually terminate the process. Thus obstacles placed in the tube [1, 5–10, 12] appear to be an essential factor in order to overcome the loss and consequently support the DDT. It is generally believed that these obstacles generate stronger turbulence, which increases the burning rate and facilitates the flame acceleration.

However, in our recent work [17] we have demonstrated that the obstacles play a more important role than just producing turbulence, in that they provide a specific physical mechanism of flame acceleration that is quali-

tatively different from the Shelkin mechanism. This new mechanism is extra strong, providing flame acceleration that is independent of the Reynolds number, through the tube width, and as such may be quite important for technical applications. Specifically, flame propagation in an obstructed channel creates pockets of fresh fuel mixture between the obstacles, as shown in Fig. 1. Gas expansion due to delayed burning in the pockets produces a powerful jet flow in the unobstructed part of the channel. The jet flow renders the flame tip to propagate much faster, which produces new pockets, generates a positive feedback between the flame and the flow, and leads to flame acceleration. The accelerating flame reaches supersonic speed with respect to the tube wall, and consequently triggers explosion and detonation.

The present paper extends the work of Bychkov et al., Ref. [17], in which the basic concepts of the new mechanism were outlined, by presenting details of the theory and simulations. Specifically, we discuss the influence of the planar/axisymmetric flow geometry and gas compression on the acceleration rate. We show that the flame accelerates much faster in cylindrical tubes than in planar channels, and that the acceleration is slowed down due to gas compression. Furthermore, as the Mach number of the flow increases, the acceleration process saturates to statistically steady flame propagation at supersonic speed with respect to the tube wall. This saturation state may develop prior to the attainment of explosion and then detonation. The flame speed in this state may be correlated with the Chapman-Jouguet (CJ) deflagration speed [18–20] and with the state of fast flames observed experimentally [6, 21]. Finally, we demonstrate numerically that flame acceleration may lead to explosion and detonation triggering.

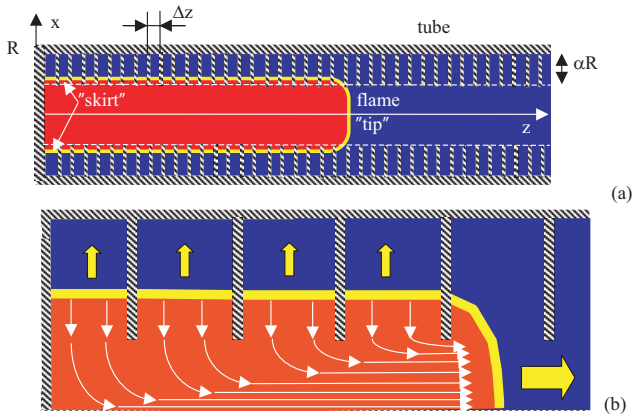


FIG. 1: Flame propagation in a channel with obstacles (a) and the jet generation mechanism (b).

2. THEORY OF FLAME ACCELERATION

Figure 1 is a schematic of the problem under study. The flame propagates from the closed end of a semi-infinite channel of half-width (radius) R , with a fraction $\alpha < 1$ blocked by obstacles. The central part of the channel, of half-width $(1 - \alpha)R$, is unobstructed. The flame propagates extremely fast along the unobstructed part of the channel, leaving behind pockets of unburned mixture, between the obstacles, which will be burned later. The deep narrow spaces between the obstacles, namely the pockets, act as mini-channels in which the flame can be considered to propagate mainly in the radial direction. This assumption is most appropriate when the obstacles are placed close to each other with deep pockets, $\Delta z \ll \alpha R$, and with slip boundary conditions at the wall. In general, burning in the pockets depends on the obstacle geometry, whose influence will be discussed later. We nevertheless recognize qualitatively the same mechanism of flame acceleration in simulations and experiments involving complicated obstacle shapes [9, 10, 12].

We now briefly state the fundamental concepts of the new mechanism presented in Ref. [17]. We employ the standard model of an infinitesimally thin flame front propagating normally to itself with the unstretched laminar flame velocity U_f . The tube wall is ideally slip and adiabatic. Non-slip boundary condition is not needed for flame acceleration in the new mechanism and the Reynolds number is not involved in the calculations. At the initial stage of flame acceleration, the flow may be treated as incompressible,

$$\nabla \cdot \mathbf{u} = 0, \quad (1)$$

while the fresh gas trapped in the pockets is burning. Expansion of the burnt gas is characterized by the density ratio of the fuel mixture and the burnt gas, $\Theta = \rho_f / \rho_b$, which is quite large for most flames, with $\Theta = 5 - 8$. In

the model of a planar laminar flame front in the pockets, the fuel mixture in a pocket is at rest, while the burnt gas is pushed out with the velocity $(\Theta - 1)U_f$, see Fig. 1 (b). This value determines the gas velocity at the border of the unobstructed part of the channel

$$|u_x| = (\Theta - 1)U_f \quad \text{at} \quad x = \pm(1 - \alpha)R. \quad (2)$$

The shape of the flame tip is of minor importance for the present mechanism, and it may be taken to be planar at all times. Consequently, the flow of the burnt gas in the unobstructed channel part is potential. Accounting for boundary condition (2), we find the flow velocity

$$(u_x; u_z) = \frac{(\Theta - 1)U_f}{(1 - \alpha)R}(-x; z). \quad (3)$$

The propagation speed of the infinitesimally thin flame front with respect to the burnt gas is

$$\frac{dZ_f}{dt} - u_z(Z_f) = \Theta U_f. \quad (4)$$

Using the velocity distribution (3), we find

$$\frac{dZ_f}{dt} = \frac{(\Theta - 1)U_f}{(1 - \alpha)R} Z_f + \Theta U_f. \quad (5)$$

Integrating Eq. (5) with the initial condition $Z_f(0) = 0$, we obtain a strong exponential acceleration of the flame tip

$$\frac{Z_f}{(1 - \alpha)R} = \frac{\Theta}{\Theta - 1} [\exp(\sigma U_f t / R) - 1], \quad (6)$$

with the scaled acceleration rate

$$\sigma = \frac{\Theta - 1}{1 - \alpha}. \quad (7)$$

The derivation of Eqs. (3) – (7) explains the basis of the new acceleration mechanism presented in Ref. [17]. This mechanism is quite powerful, with the acceleration rate (7) much larger than that of the Shelkin mechanism in smooth tubes [14]. The scaled acceleration rate does not depend on the Reynolds number, and hence the viscosity and the tube width. As will be discussed below, viscosity and turbulence may induce supplementary effects in the new acceleration mechanism. As pointed out in Ref. [17], this new acceleration mechanism has many features in common with the acceleration of finger flames, Refs. [22, 23], although the finger flame acceleration is quite limited in time, yielding maximum increase in the burning rate by a factor of only 10-15 relative to the planar flame speed [23]. In contrast, the new physical mechanism leads to supersonic flame propagation with respect to the tube wall, with possible transition to explosion and detonation. It was also demonstrated in Ref. [17] that the new mechanism remains effective even when the flame skirt touches the main wall of the channel.

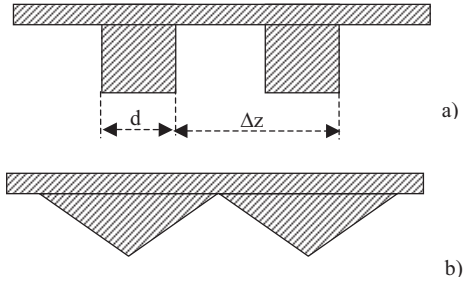


FIG. 2: Typical obstacle shapes discussed in ICDERS-2007.

Theoretical understanding of the new acceleration mechanism enables the analysis of the optimal obstacle geometry for flame acceleration. Figure 2 shows typical obstacle shapes discussed in Refs. [9–13]. Specifically, in Fig. 2 (a) we have rectangular obstacles of thickness d and spacing Δz . In this case delayed burning occurs only between the obstacles, while the volume occupied by an obstacle itself is ineffective for flame acceleration. Averaging volume production in the burning process over the obstacle step, we rewrite the boundary condition (2) as

$$|\langle u_x \rangle| = (1 - d/\Delta z)(\Theta - 1)U_f \text{ at } x = \pm(1 - \alpha)R, \quad (8)$$

which leads to the reduced acceleration rate

$$\sigma = (1 - d/\Delta z) \frac{\Theta - 1}{1 - \alpha}. \quad (9)$$

Thus, thinner obstacles produce stronger acceleration. Another possible factor suggested was obstacle phase shift at the bottom of the channel in comparison to that at the top. This suggestion, however, is not expected to substantially affect the laminar flame dynamics, although it could influence the turbulence generated in the flow in later stages. The triangular obstacle shape in Fig. 2 (b) also renders the flame acceleration slower because it reduces the volume of the fresh fuel mixture trapped between the obstacles. Consequently, the optimal design for flame acceleration is that of the infinitely thin obstacles shown in Fig. 1. For a fixed tube radius R , maximum acceleration rate is achieved for maximum possible blockage ratio, i.e. for minimum value of $(1 - \alpha)R$. However, for a fixed width of the free channel part $(1 - \alpha)R$, the acceleration rate does not depend on the total tube radius R , i.e. it does not depend on the depth of the pockets. This is true, of course, only when pockets are sufficiently deep with α comparable to unity. Very small obstacles ($\alpha \ll 1$) cannot be treated as obstacles and the new mechanism is ineffective. Still, typical experimental configurations employ obstacles with the blockage ratio of $1/4 < \alpha < 3/4$, for which the present mechanism is quite effective. The dimensional acceleration rate $(\Theta - 1)U_f/R(1 - \alpha)$ is determined by the expansion factor Θ , the laminar flame velocity U_f and the half-width of the unobstructed channel part $R(1 - \alpha)$. The theoretical

model of a laminar flow does not predict any dependence of the acceleration rate on the spacing between the obstacles. As we shall demonstrate numerically in Sec. 4, the spacing between the obstacles determines primarily the amplitude of the velocity pulsations (see also Ref. [17]). Still, these pulsations do not change the average acceleration rate, which remains quite close to the predictions of the theoretical model.

Additional increase in the acceleration rate is realized in the axisymmetric geometry. Here we consider an axisymmetric tube with obstacles in the form of planar rings blocking the space $(1 - \alpha)R < r < R$ similar to Fig. 1. Suppose the flame tip accelerates as $Z_f = Z_f(t)$. A pocket between the obstacles at the position z starts burning at the instant $t_f(z)$, where $t_f(z)$ is the inverted function $Z_f(t)$. The flame in the axisymmetric pockets expands with the radius growing as

$$R_f = (1 - \alpha)R + U_f[t - t_f(z)]. \quad (10)$$

The radial velocity at the exit of the pocket, at $r = (1 - \alpha)R$, is given for an incompressible flow as

$$(\Theta - 1)R_f U_f = -(1 - \alpha)R u_r, \quad (11)$$

which determines the boundary condition at the border of the unobstructed part of the channel $r = (1 - \alpha)R$,

$$u_r = -(\Theta - 1)U_f \left(1 + \frac{U_f}{(1 - \alpha)R} [t - t_f(z)] \right). \quad (12)$$

In the event of exponential, or near-exponential, flame acceleration

$$Z_f = Z_0 [\exp(\sigma U_f t / R) - 1], \quad (13)$$

the instant $t_f(z)$ varies logarithmically, and hence slowly, with z , as

$$t_f = \frac{R}{\sigma U_f} \ln(z/Z_0 + 1), \quad (14)$$

where Z_0 is some amplitude.

Let us first determine the flame acceleration neglecting the increase in the flame radius R_f of Eq. (10) in comparison with $(1 - \alpha)R$. Then, the axisymmetric solution to the continuity equation (1) in the unobstructed part of the channel is

$$(u_r; u_z) = \frac{(\Theta - 1)U_f}{(1 - \alpha)R} (-r; 2z), \quad (15)$$

which is the axisymmetric counterpart of Eq. (3). The solution (4) – (7) is respectively modified in the axisymmetric geometry as

$$\frac{dZ_f}{dt} = 2 \frac{(\Theta - 1)U_f}{(1 - \alpha)R} Z_f + \Theta U_f, \quad (16)$$

with

$$\frac{Z_f}{(1-\alpha)R} = \frac{\Theta}{2(\Theta-1)} [\exp(\sigma U_f t/R) - 1], \quad (17)$$

and

$$\sigma = 2 \frac{\Theta - 1}{1 - \alpha}. \quad (18)$$

Equation (18) shows that flame acceleration in the axisymmetric geometry is twice that in the planar case.

We next account for the increase in R_f as compared to $(1-\alpha)R$. Taking the radial velocity component in the same form as in Eq. (15),

$$u_r = -\frac{(\Theta-1)U_f}{(1-\alpha)R} r \left(1 + \frac{U_f}{(1-\alpha)R} [t - t_f(z)] \right), \quad (19)$$

we find the respective z-velocity component

$$u_z = 2 \frac{(\Theta-1)U_f}{(1-\alpha)R} \left(z + \frac{U_f}{(1-\alpha)R} \int [t - t_f(z)] dz \right), \quad (20)$$

and its value at the flame tip

$$u_z = 2 \frac{(\Theta-1)U_f}{(1-\alpha)R} Z_f \left(1 + \frac{U_f}{(1-\alpha)R} \langle t - t_f(z) \rangle \right), \quad (21)$$

where

$$\langle t - t_f(z) \rangle = t - \frac{1}{Z_f} \int_0^{z_f} t_f(z) dz. \quad (22)$$

When the fuel mixture in the first pocket is almost completely burnt, accounting for Eqs. (14), (17), the averaging in Eq. (22) yields

$$\sigma_0 \frac{U_f}{R} \langle t - t_f(z) \rangle = 1 - \frac{Z_0}{Z_f} \ln \left(\frac{Z_f}{Z_0} + 1 \right), \quad (23)$$

where σ_0 is given by Eq. (18). The second term in Eq. (23) diminishes asymptotically to zero with time, but the first term leads to corrections to Eqs. (16), (18) as

$$\frac{dZ_f}{dt} = 2 \frac{(\Theta-1)U_f}{(1-\alpha)R} \left(1 + \frac{1}{2(\Theta-1)} \right) Z_f + \Theta U_f, \quad (24)$$

and

$$\sigma = 2 \frac{\Theta - 1}{1 - \alpha} \left(1 + \frac{1}{2(\Theta - 1)} \right). \quad (25)$$

The second term in Eq. (25) may be treated as corrections to the first one in the limit of $2(\Theta-1) \gg 1$, which holds with good accuracy of about 7% for realistic fuel mixtures. Furthermore, this correction becomes important only when the leading part of the flame skirt has almost touched the main wall, when burning in the first

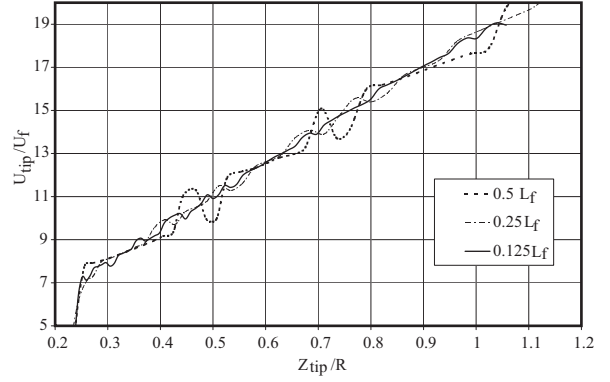


FIG. 3: Resolution test: flame tip velocity versus tip position for $Ma = 0.001$, $\alpha = 1/2$ and various mesh sizes (0.125; 0.25; 0.5) L_f .

pocket is almost finished. At the beginning of the burning process, the acceleration rate should be approximated by Eq. (18). However, even during this initial period of flame acceleration, the flame velocity may attain fairly large values relative to the sound speed, at which the incompressibility assumption fails. Thus, the flame acceleration rate should be evaluated by Eq. (18) rather than Eq. (25).

The theory above constitutes the backbone of the new mechanism of extremely fast flame acceleration in tubes/channels with obstacles. Still, this theory may be developed further to incorporate other effects, such as gas compression, viscosity, non-slip at the wall, etc, which also influence the acceleration process. Here, we discuss briefly some of these effects.

(1) Gas compression: The present theory is developed for incompressible flows. Compressibility is expected to moderate the flame acceleration considerably by recognizing that the flame velocity is limited by the CJ deflagration value. Preliminary numerical results on this subject are given in Ref. [17], and similar effects for smooth tubes are also discussed in Ref. [20]. We shall perform additional modeling later to demonstrate the role of gas compression.

(2) Curved flame shape in the pockets and at non-slip wall: Flame shape in the pockets is not necessarily planar, as we assumed in the calculations. Inclined or curved flame shapes provide faster propagation of the front and stronger cumulative expansion. A flame may acquire a curved shape because of intrinsic instabilities, viscous effects, etc. For example, the viscosity and non-slip wall can increase the flame speed by a factor of about 1.5 [24]. The curved flame shape in the pockets renders acceleration of the flame tip stronger. In such cases the planar flame velocity in Eq. (2) should be multiplied by some factor describing the increase in the flame velocity in the pockets.

(3) Turbulence in the pockets: Flow in the unob-

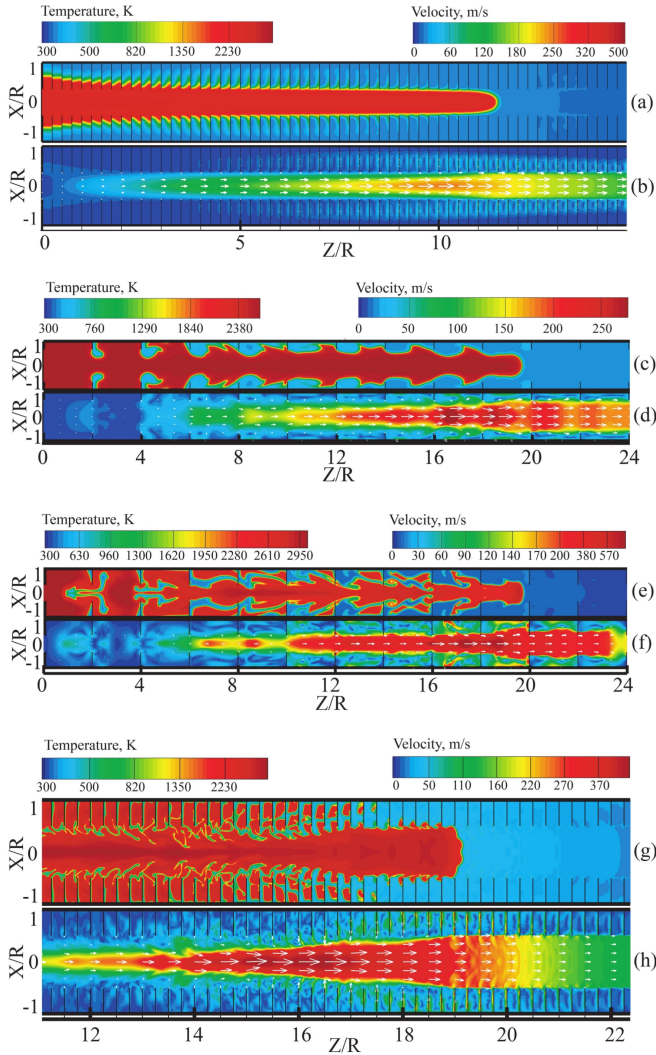


FIG. 4: Snapshots of temperature and velocity in the flow generated by an accelerating flame in the planar geometry for the following parameters: (a, b) $Ma = 0.001$, $\Delta z/R = 1/4$, $\alpha = 2/3$ (appears in [17]); (c, d) $Ma = 0.005$, $\Delta z/R = 2$, $\alpha = 1/3$; (e, f) $Ma = 0.005$, $\Delta z/R = 2$, $\alpha = 2/3$; (g, h) $Ma = 0.001$, $\Delta z/R = 1/4$, $\alpha = 1/2$ (appears in [17]).

structured part of the channel pushed by the accelerating flame also generates turbulence in the pockets, see, for example, [6, 10, 17]. Turbulence corrugates the flame front and increases the burning rate in the pockets. The effect of turbulence becomes especially noticeable when the distance between the obstacles is comparable to or larger than the obstacle size, $\Delta z \propto \alpha R$.

(4) Large spacing between the obstacles: Large spacing Δz causes two competing effects. On the one hand, the flow in the unobstructed part of the channel becomes less confined, which may be interpreted as decreased effective blockage ratio and thereby reduces the acceleration rate. On the other hand, large spacing leads to stronger turbulence in the pockets thus augmenting flame acceleration.

Numerical simulation [17] showed that these effects compensate each other at moderate values of $\Delta z/R = 1, 2$, with turbulence having a slightly stronger effect in the developed stage of flame acceleration.

(5) Loss to the wall: In smooth tubes heat loss to the wall reduces expansion of the burning gas dramatically and slows down flame acceleration. However, in tubes with sufficiently deep and thin obstacles this negative influence may be reduced considerably. Indeed, thin obstacles may be heated rapidly and do not extract much energy from the flow. At the same time, loss to the main wall is minimized since it is mostly in contact with the fresh fuel mixture instead of the burnt gas. One should expect that loss to the main wall is equivalent to an effective smaller radius of the tube, $R_{eff} < R$, but with the same size of the unobstructed part of the channel $(1 - \alpha)R$. Since the acceleration rate is determined by $(1 - \alpha)R$, not by R , then one should expect minimal influence of the loss in such a configuration.

3. BASIC EQUATIONS AND NUMERICAL METHOD

We performed direct numerical simulation of the hydrodynamic and combustion equations including transport processes and Arrhenius kinetics. Both 2D planar and axisymmetric cylindrical flows were investigated using the Navier-Stokes system of the governing equations presented, e.g., in Refs. [14, 15]. To avoid the thermal-diffusive instability we took unity Lewis number $Le = 1$, with $Pr = 0.75$ and the dynamical viscosity $\mu = 1.7 \times 10^{-5} \text{Ns/m}^2$. The fuel-air mixture and burnt gas were assumed to be a perfect gas with a constant molar mass $m = 2.9 \times 10^{-2} \text{kg/mol}$. We considered a one-step irreversible Arrhenius reaction with an activation energy E_a , pre-exponential factor of inverse time dimension τ_R^{-1} , first order dependence on concentration of the fuel mixture, and first or second order dependence on density similar to Ref. [26]. The first order was used in all studies of flame acceleration and saturation to the CJ state. The second order was employed to obtain explosion and transition to detonation, since in that case flame dynamics is much more sensitive to pressure and temperature build-up in the compression waves generated by an accelerating flame. In the simulations we took $E/R_p T_f = 32$ in order to have better resolution of the reaction zone. In the present study we focus mainly on the flame acceleration and preheating of the fuel mixture ahead of the flame front, which do not depend on the activation energy. The activation energy is crucial for time and position of explosion triggering and DDT. However, proper *quantitative* investigation of DDT cannot be performed within a simplified one-step mechanism of chemical reaction kinetics. Instead, it requires separate description of the chemical kinetics at high temperatures

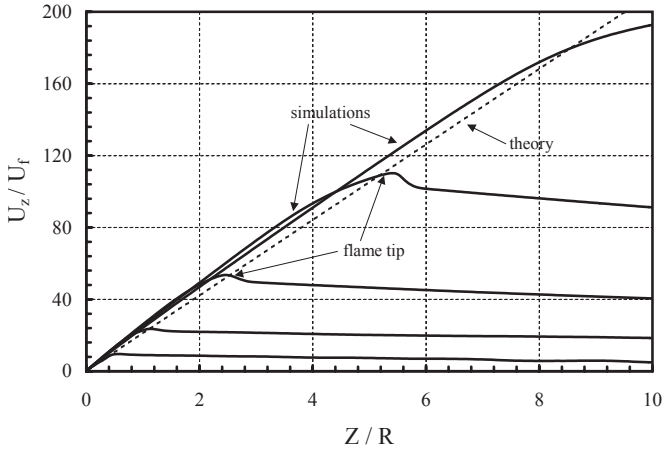


FIG. 5: Profile of the scaled z -velocity along the channel axis plotted for $\alpha = 2/3$, $Ma = 0.001$, $\Delta z/R = 1/4$ at the time instants $U_f t/R = 0.02 - 0.16$ equally spaced in time. The theoretical line is related to Eq. (4).

(flame, detonation) and low temperatures (explosion ignition). For this reason, in the present work we perform only qualitative study of explosion triggering choosing a scaled activation energy convenient for such a study. The factor τ_R was adjusted to obtain a particular value of the planar flame velocity U_f by solving the associated eigenvalue problem [27, 28]. For example, taking the planar flame velocity $U_f = 34.7$ cm/s, we set $\tau_R = 4.06 \cdot 10^{-8}$ s for the first-order reaction. The flame thickness is conventionally defined as

$$L_f \equiv \frac{\mu_f}{\text{Pr} \rho_f U_f}, \quad (26)$$

where $\rho_f = 1.16$ kg/m³ is the unburnt mixture density. We took initial temperature of the fuel mixture $T_f = 300$ K, initial pressure $P_f = 10^5$ Pa, adiabatic index $\gamma = 1.4$, and initial expansion ratio $\Theta = 8$. We took different values of the initial Mach number in the range $10^{-3} \leq Ma \equiv U_f/c_s \leq 10^{-2}$, with the lower limit corresponding to realistic methane and propane flames. By varying the Mach number, we investigated the influence of gas compression on flame acceleration. The theory of Sec. 2 does not involve the Reynolds number, which implies minor dependence of the results on the channel/tube width, provided it is sufficiently large. On the other hand, simulation of burning in wide channels with obstacles can be quite time consuming. For this reason, in the simulations we used a moderate value of the channel half-width (radius), $R = 24L_f$. Some of the 2D planar simulation runs were performed only for half of the channel assuming symmetry. However, the majority of runs were for the entire channel, which is especially important for the developed stages of flame acceleration involving turbulence as well as for explosion triggering.

The present modeling is also relevant to combustion in micro-channels, which is a rapidly developing subject.

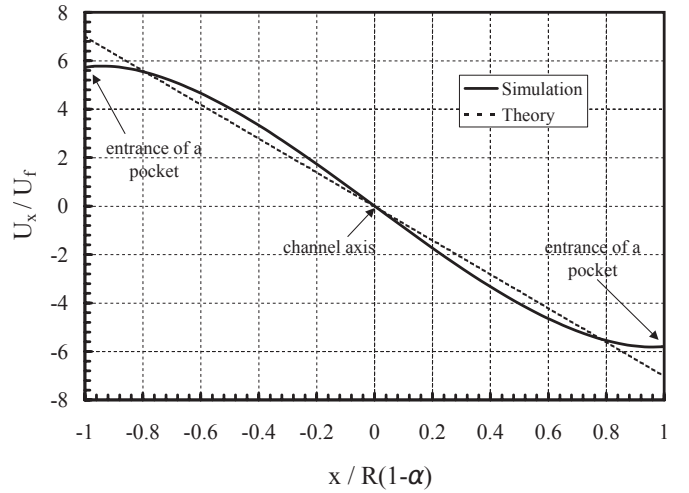


FIG. 6: Profile of the scaled x -velocity along the cross-section $z/R = 0.5$ plotted for $\alpha = 2/3$, $Ma = 0.001$, $\Delta z/R = 1/4$ at the time instant $U_f t/R = 0.16$. The theoretical line is related to Eq. (4).

Recent theory, modeling and experiments [14–16] demonstrated the possibility of DDT in smooth micro-tubes. The present results also successfully predict flame acceleration and DDT in micro-channels with obstacles, while recognizing that the present analysis of course has a wider implementation than micro-channel flows. According to the theory of Sec. 2, the same extra-strong mechanism of flame acceleration works even in very wide tubes, though it is impossible to attain such a state in numerical simulations at present because of the inevitable computational limitations. The channel width employed in the present simulation determines the Reynolds number related to the laminar flame speed $Re = U_f R/\nu = R/L_f \text{Pr} = 32$. The Reynolds number related to the flow $Re = \langle u_z \rangle 2R/\nu$ can be larger by several orders of magnitude due to flame acceleration and thermal expansion of the burnt gas. Flame acceleration and increase in the Reynolds number may produce turbulence in the flow. Indeed, our simulation shows that the burning happens in the laminar regime at the beginning of flame acceleration, and considerable turbulence is generated close to the end of the process. Turbulence level depends typically on the obstacle spacing.

We took slip and adiabatic boundary conditions at the tube wall:

$$\mathbf{n} \cdot \mathbf{u} = 0, \quad \mathbf{n} \cdot \nabla T = 0, \quad (27)$$

where \mathbf{n} is the unit normal vector at the wall. At the open end of the channel, non-reflecting boundary conditions were used. As initial conditions, we used a hemisphere of hot "burnt" gas at the channel axis at the closed end of the tube, with the temperature profile given by the analytical solution of Zel'dovich and Frank-

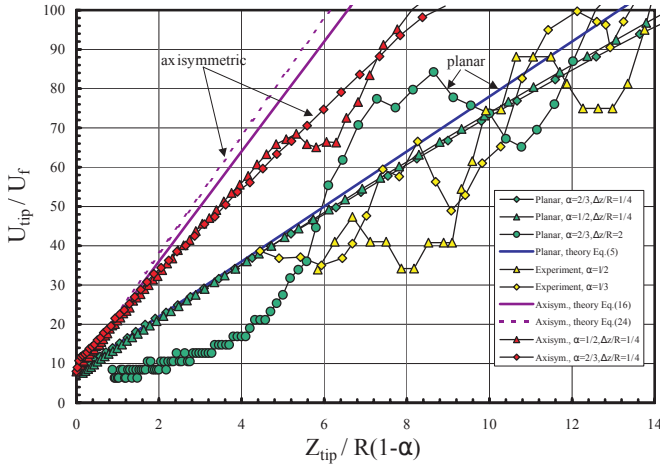


FIG. 7: Scaled velocity of the flame tip versus the scaled tip position for planar and axisymmetric geometry. The theoretical lines correspond to Eqs. (5), (16), (24). The symbols show results of numerical modeling for $\alpha = 1/2; 2/3$ and $\Delta z/R = 1/4; 2$. The experimental data shows results of Ref. [11].

Kamenetskii [2, 25],

$$T = T_f + (T_b - T_f) \exp\left(-\frac{\sqrt{x^2 + z^2}}{L_f}\right) \text{ if } z^2 + x^2 < r_f^2,$$

$$T = \Theta T_f \text{ if } z^2 + x^2 > r_f^2,$$

$$Y = (T_b - T)/(T_b - T_f), P = P_f, u_x = 0, u_z = 0. \quad (28)$$

Here r_f is the radius of the hemisphere. The boundary of the hot gas is not a flame front yet, and we take both cold and hot gas initially at rest. The finite initial radius r_f is equivalent to a time shift, which requires proper adjustments when comparing the theory and numerical simulations. When necessary, we shifted the numerical solution in time to have the theory and the modeling results starting at the same point.

A 2D hydrodynamic Navier-Stokes code adapted for

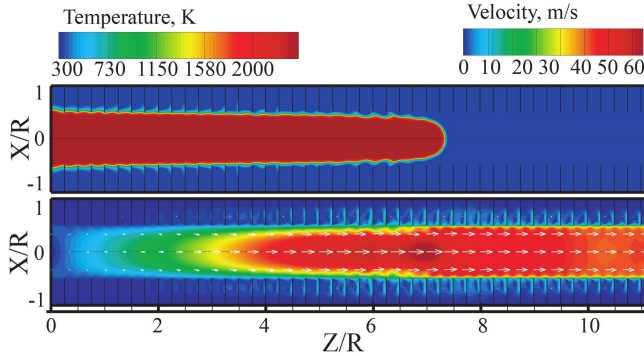


FIG. 8: Snapshots of temperature and velocity in the flow generated by an accelerating flame in an axisymmetric geometry for $Ma = 0.001$, $\Delta z/R = 1/4$; $\alpha = 1/2$.

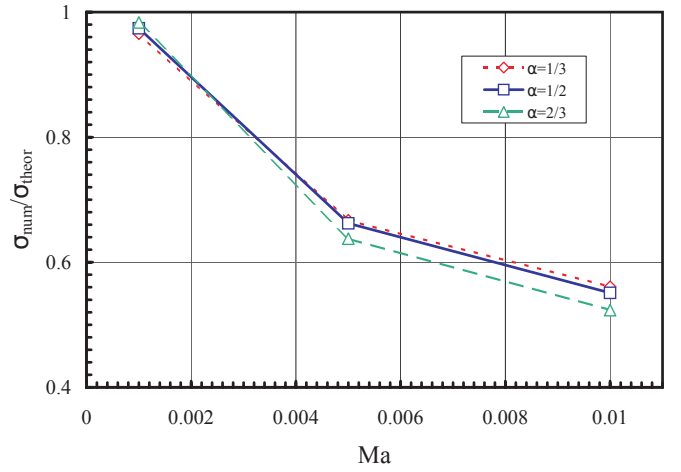


FIG. 9: Ratio of the acceleration rate obtained numerically to predicted theoretically, Eq. (7), versus the initial Mach number for the planar geometry and $\alpha = 1/3; 1/2; 2/3$ and $\Delta z/R = 1/4$.

parallel computation [29–31] was used. The numerical scheme is second-order accurate in time, fourth order in space for the convective terms, and second order in space for the diffusive terms. The code is robust and accurate, having been successfully used in combustion and aero-acoustic applications. The code is available in 2D (Cartesian and cylindrical axisymmetric) and 3D Cartesian versions. In the present work, we performed only 2D simulations to save computational time and to be able to perform a large number of simulation runs required for a thorough investigation of the problem.

A uniform grid with quadratic cells of size $0.2L_f$ was used to ensure isotropic propagation of the curved flame in x and y directions. The longitudinal size of the calculation domain changes dynamically, following the leading pressure wave. Splines of the third order were used for re-interpolation of the flow variables during periodic grid reconstruction to preserve second-order accuracy of the numerical scheme. We performed several test simulation runs with resolutions of $0.125L_f$, $0.25L_f$, $0.5L_f$. The test demonstrated that the flame velocity grows exponentially for all chosen resolutions, with the difference in the scaled acceleration rate σ not exceeding 6%. The dependence of the scaled flame tip velocity U_{tip}/U_f on the scaled distance Z_{tip}/R is shown in Fig. 3 for different resolutions. Resolution tests also showed convergence of the acceleration rate σ value with increasing resolution.

4. SIMULATION RESULTS AND DISCUSSION

Simulation of the flame acceleration in channels/tubes with obstacles was performed at various flow parameters. In particular, we used various blockage ratios $\alpha = 1/3; 1/2; 2/3$, various spacings between the ob-

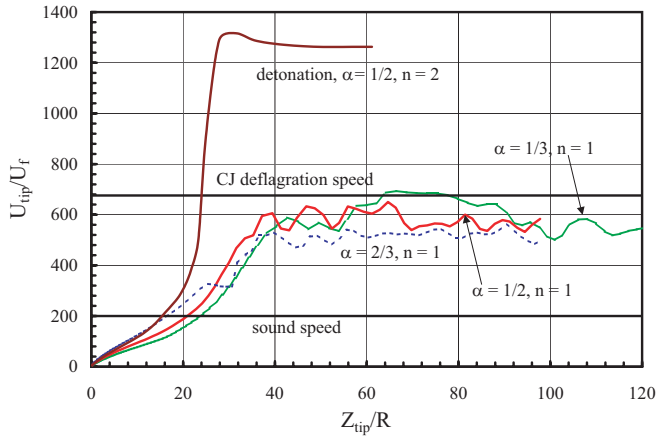


FIG. 10: Scaled velocity of the flame tip versus tip position for the planar geometry and $\alpha = 1/3; 1/2; 2/3$, $\Delta z/R = 1/4$, and different reaction order with respect to density $n = 1, 2$. The plot with $n = 2$ shows also transition to detonation.

stacles, $\Delta z/R = 1/4; 1/2; 1; 2$, and various initial Mach numbers. Figure 4 shows the characteristic flame shape and flow velocity obtained at various conditions. It is found that, in spite of these differences, all snapshots demonstrate the same basic feature of flame acceleration in channels with obstacles described theoretically in Sec. 2, namely, the flame tip propagates fast along the unobstructed part of the channel, leaving pockets of unburned fuel mixture in between the obstacles. Delayed burning between the obstacles involves various levels of turbulence created by the flow. In Fig. 4 (a) the flow is laminar, and this regime is quite similar to the theoretical one sketched in Fig. 1 and described in Sec. 2. In contrast, Fig. 4 (g) shows rather strong turbulence corresponding to the developed stage of flame acceleration. Figures 4 (c, e) show the flame shape for relatively large obstacle spacing: the snapshots are similar to the experimental photos of accelerating flames in Ref. [10]. We also observe a strong jet-flow developing in the unobstructed part of the channel in Fig. 4 (b, d, f, h) which is an important part of the acceleration mechanism described in Sec. 2. Figure 5 shows the z -velocity component of the jet along the channel axis for the initial laminar stages of burning. As predicted by the theory, Eq. (4), plotted by the dashed line, we observe almost linear increase of the gas velocity from the closed end of the tube to the flame tip. The x -velocity component in Fig. 6 also demonstrates good agreement between the theory and simulation. Comparison of the theory and simulation in Figs. 5, 6 supports the potential flow model in the burnt gas employed in the analytical theory of Sec. 2 and of Ref. [17]. The slight deviation between the theoretical and numerical results is due to the finite flame thickness and viscosity employed in the simulation. For example, because of viscous friction, the z -velocity component in the simulation inevitably decreases at the border between the

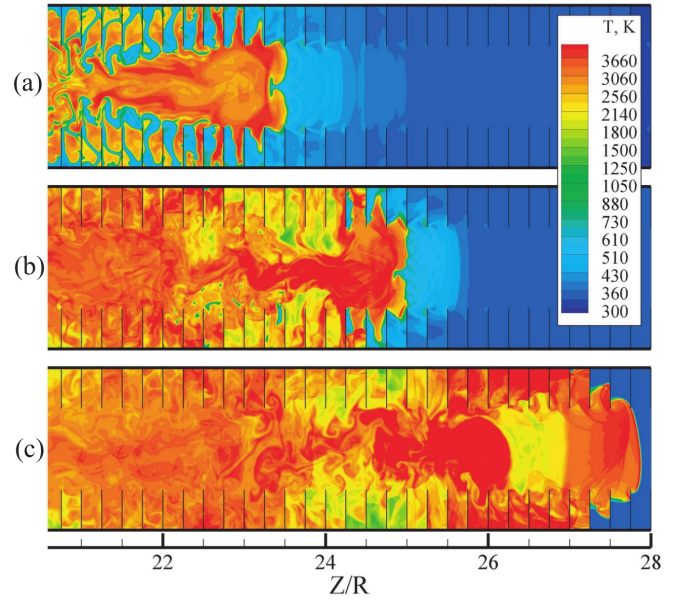


FIG. 11: Temperature field for three consecutive moments during deflagration-to-detonation transition for the second-order reaction for $\Theta = 8$, $Ma = 0.005$, $\Delta z/R = 1/4$, $\alpha = 1/2$.

obstructed and unobstructed parts of the channel, which produces vorticity in that region as shown in Fig. 1 (c) of Ref. [17]. Another interesting question is related to the vorticity generated at the curved flame front as predicted by the classical theory [2]. In the present case the curved shape of the flame tip plays a minor role in the flame dynamics in comparison with the powerful acceleration mechanism described in Sec. 2. For example, replacing the curved flame tip by a planar one in Fig. 4 (a), we obtained negligible change of the total flame surface area as well as the total burning rate. Similarly, the vorticity generated by the curved flame tip plays a minor role in comparison with the strong jet flow described in Sec. 2 and with the vorticity generated in that flow because of viscous forces. In this sense the present problem is completely different from, say, the Darrieus-Landau instability for which a curved flame shape and the flame velocity increase are intrinsically related to the vorticity production [32].

One of the most interesting questions in this study is to identify how the flame acceleration depends on the obstacle parameters: blockage ratio and spacing, i.e. pocket depth and width. According to the theory of Sec. 2, the acceleration rate is determined by the size of the unobstructed part of the channel, $R(1 - \alpha)$. In the theoretical model, the pocket depth and width do not influence the acceleration, provided that the depth is not too small and the width is not too large, for which the notion of a pocket becomes meaningless. Taking proper scaling of the tip position $Z_f/R(1 - \alpha)$, we observe that the numerical results reproduce the theoretical predictions for different

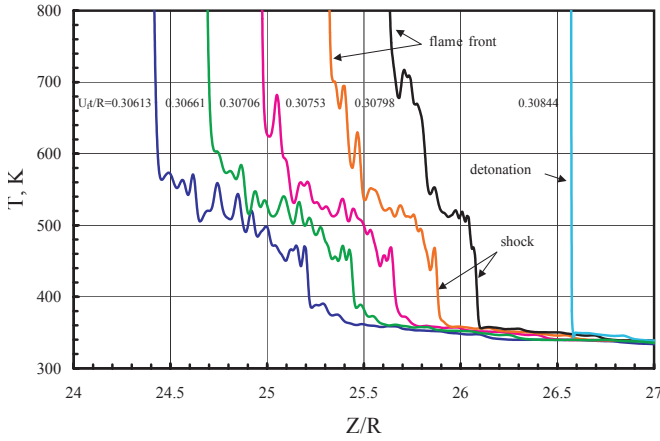


FIG. 12: Temperature profiles along the channel axis at different time instants close to the instant of detonation triggering; other parameters are the same as for Fig. 11.

obstacle parameters, see Fig. 7. Additional numerical data, which is not presented in Fig. 7 to avoid clutter, can be found in Ref. [17]. In the event of small spacing between the obstacles ($\Delta z/R = 1/4$), the flame tip accelerates monotonically as described by the theoretical model. When the spacing is considerable ($\Delta z/R = 2$), we observe strong turbulent pulsations with space period well-correlated with the distance between the obstacles. Still, even in this case, the average velocity of the flame tip is predicted by the theory of Sec. 2 with good accuracy. Figure 7 also shows good agreement of the theory and simulation with the experimental results [11], which also demonstrate noticeable velocity pulsations because of the large spacing between the obstacles. When compared to the obstacle positions (not shown in the figure because of the chosen scaling), both simulation and experiment demonstrate an increase in the flame tip velocity at every obstacle. Maximum pulsation velocity corresponds approximately to the middle between two obstacles.

For the axisymmetric geometry, the theory of Sec. 2 predicts considerably stronger flame acceleration as compared to the planar case. Figure 7 shows the velocity of the flame tip versus the position in the tube for $Ma = 10^{-3}$, $\alpha = 1/2$; $2/3$, and demonstrates much faster flame acceleration. The growth rate is about twice larger in agreement with Eqs. (16), (18). However, quantitative agreement between the theory and simulation in the axisymmetric case is not as good as in the planar geometry. In the planar case of Fig. 7, the quantitative difference is less than 5%, while in the axisymmetric case this difference increases from about 10% at the beginning to 20% at later time. Equation (18) provides better agreement with the simulation than Eq. (25), which may indicate a minor role of the radius growth for the flame skirt in the pockets. This effect may be observed directly for the flame shape in the axisymmetric geometry shown in

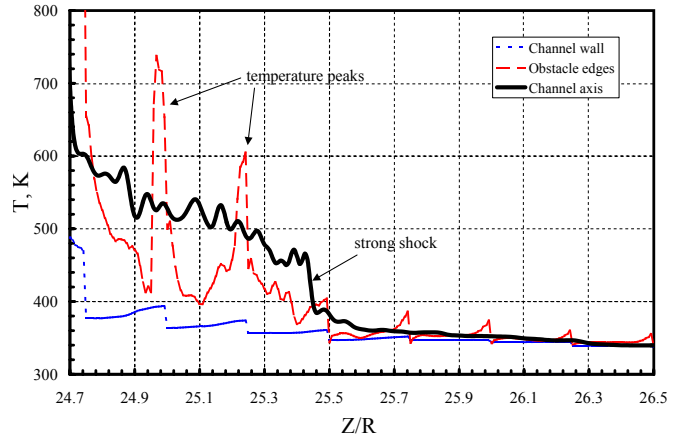


FIG. 13: Temperature profiles along the channel axis, at the obstacle edges and at the wall for $U_{ft}/R = 0.30661$; other parameters are the same as for Fig. 11.

Fig. 8, which shows that even minor penetration of the flame skirt into the pockets between the obstacles provides quite strong flame acceleration in the axisymmetric geometry. For comparison, the flame skirt penetrates much deeper into the pockets in the planar case of Fig. 4 (a). We also observe that the difference between theory and modeling becomes larger in Fig. 7 as the flame velocity increases. The quantitative difference of 10-20% in the axisymmetric case is partly related to the influence of viscosity and the moderate tube width, corresponding to moderate values of the Reynolds number. As obtained in numerical studies of the early acceleration of finger flames [23], moderate tube width reduces flame acceleration as compared to the theory. However, there are also other reasons that cause a reduction of the flame acceleration in the numerical modeling. The first is the incompressibility assumption of the theory. This assumption is acceptable at the beginning of the acceleration, but deteriorates as the local Mach number increases as the flame accelerates. The deviation develops faster for the axisymmetric geometry because of its faster acceleration. In order to study the influence of gas compression on the flame acceleration, we investigated the dependence of the scaled acceleration rate σ on the initial Mach number, as shown in Fig. 9 for various values of the blockage ratio. It is thus seen that the scaled acceleration rate decreases strongly with the Mach number. For initial Mach number $Ma = 10^{-2}$ instead of $Ma = 10^{-3}$, the acceleration rate is approximately reduced by a factor of two.

The slowdown of flame acceleration because of gas compression agrees with the concept that the flame propagation velocity cannot exceed the value of the Chapman-Jouguet (CJ) limiting state, for which the downstream flow is sonic. We therefore expect saturation of the flame tip velocity to a certain steady value at the end of the acceleration process, but prior to an explosion. Indeed, Fig. 10 demonstrates for the planar geometry such a saturat-

tion, obtained in the numerical simulation at the final stage of flame acceleration, for various blockage ratios. The initial Mach number in Fig. 10 is $Ma = 5 \cdot 10^{-3}$, and the saturation velocity is about $(2.5 - 3.0)c_s$. For comparison, one-dimensional theory predicts the CJ deflagration velocity with respect to the wall in the limit of large energy release ($\Theta \gg 1$) as [18, 19]

$$\frac{U_{CJ}}{c_s} = \left[1 + \frac{\gamma(\gamma - 1)}{2(\gamma + 1)} \right] \sqrt{2 \frac{\Theta - 1}{\gamma + 1}}. \quad (29)$$

In the present case of $\gamma = 1.4$, $\Theta = 8$, Eq. (29) yields $U_{CJ} \approx 2.68c_s$, which is about the saturation velocity obtained in the present numerical simulation. More accurate theoretical calculation of the CJ deflagration velocity without the assumption of $\Theta \gg 1$ yields $U_{CJ} \approx 3.38c_s$, which is also close to the present numerical results.

Finally, we discuss how flame acceleration in channels with obstacles may lead to DDT. Since the time and position of DDT are quite sensitive to the chemical kinetics adopted, our results on detonation triggering should be considered as qualitative. At the same time, they demonstrate the general features of DDT irrespective of the particular fuel mixture. It is well known that any flame propagating from a closed end pushes a flow in the fuel mixture with a weak shock/compression wave at the head of the flow. The flame acceleration renders the compression wave stronger, until it develops into a shock of considerable amplitude. Preheating of the fuel mixture by the shock is conventionally considered as one of the main elements of DDT both in smooth tubes and in channels with obstacles [1–6]. The temperature behind the shock increases and the reaction time in any compressed gas parcel decreases drastically. The decrease in the reaction time may result in explosion and DDT ahead of the flame front unless the parcel is burnt by the flame before active explosion is initiated. Thus, in general, we may expect two possible outcomes for the flame acceleration: 1) If the reaction time behind the shock is sufficiently short, then it drives the explosion and DDT; 2) The reaction time may be longer than the interval available for a gas parcel to travel between the shock and the flame. In this case explosion does not occur and the final state of flame acceleration is the CJ deflagration. For comparison, the possibility of spontaneous explosion ahead of an accelerating flame was considered in the theory [33] for smooth tubes. Both CJ detonation and deflagration have also been found in smooth tubes experimentally in Ref. [16]. In channels with obstacles, the state of CJ deflagration is also known as "fast flames" [6, 8]. In the present simulations we observed both possibilities of DDT and CJ deflagration for different reaction kinetics. Taking reaction of the first order with respect to density (designated by $n = 1$ in Fig. 10), we obtained statistically steady CJ deflagration at the end of flame acceleration with no explosion or DDT, see Fig. 10. This result indicates that

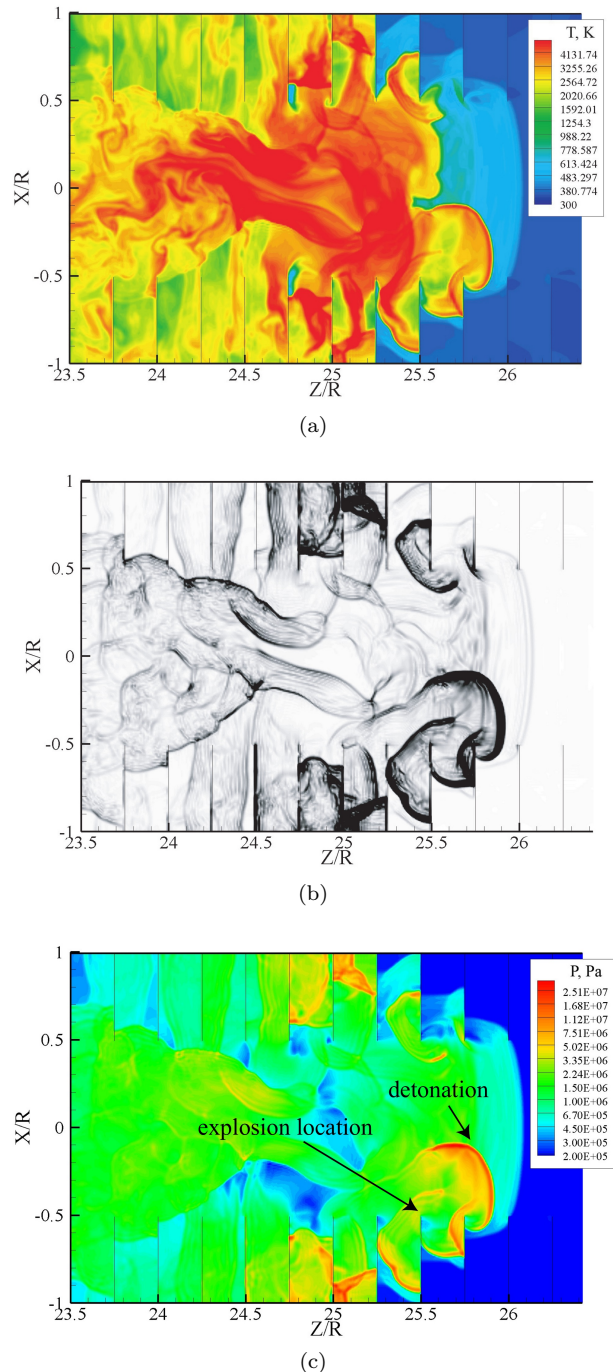


FIG. 14: (a) Temperature, (b) pressure gradient modulus and (c) pressure fields close to the point of explosion triggering for the second-order reaction for $\Theta = 8$, $Ma = 0.005$, $\Delta z/R = 1/4$, $\alpha = 1/2$.

the decrease in the reaction time behind the shock is not sufficient, and gas parcels are consumed by the flame front before spontaneous reaction develops into a powerful explosion. Thus, in order to observe DDT, we need to take another reaction mechanism, which is more sensitive to pressure and temperature increase in the shock.

Similar to Ref. [26], we considered a reaction of the second order with respect to density, $n = 2$, and obtained explosion triggering and DDT, see Fig. 10. Remarkably, in this case the reaction rate is so sensitive to pressure and temperature that the DDT occurs before the flame reaches the CJ deflagration state. Figure 11 shows characteristic temperature snapshots at the DDT. It is seen that the accelerating flame acts like a piston pushing a shock, which raises the temperature of the fuel mixture ahead of the flame, as shown in Fig. 11 (a, b). The snapshot of Fig. 11 (c) already corresponds to detonation. Development of the temperature profiles ahead of the flame front along the channel axis is shown in Fig. 12 for the time instants $U_f t/R = 0.30613 - 0.30844$ close to the DDT time. Unlike the case of smooth tube with monotonic temperature distribution in the compression wave [33], in Fig. 12 we observe noticeable temperature pulsation due to secondary shocks reflected from the obstacles. The main tendency nevertheless remains the same: we can see a considerable temperature jump in the main shock followed by further temperature increase in the compression wave from the shock to the flame front. The compression wave and the shock become stronger as the flame accelerates, until explosion starts and develops into detonation.

Recent papers [20, 34] on DDT in tubes with smooth adiabatic wall have also demonstrated the important role of viscous heating at the wall in addition to shock heating. Because of viscous heating, the temperature at the wall of a smooth adiabatic channel is larger than that at the axis, and numerical modeling demonstrates DDT onsets at the wall. A similar physical mechanism of viscous heating may also be identified in channels with obstacles, though with proper modifications due to the specific geometry. To elucidate the mechanism, Fig. 13 shows the temperature profiles for $U_f t/R = 0.30661$ along the channel axis, along the wall and at specific obstacle edges. We can see that on average, temperature is considerably higher at the channel axis. Obstacles reduce the shock strength, which results in much lower average temperature at the obstacle edges, with the lowest temperature at the wall deep in the pockets. Still, obstacles not only moderate the main shock, but they also produce hot spots, which may be crucial in explosion triggering and DDT [2, 35]. Though the average temperature is lower at the obstacle edges, we also observe sharp peaks of temperature ahead of every obstacle, which are much higher than the respective temperature at the channel axis. There are two possible reasons for these temperature peaks. First, secondary shock waves reflected from the obstacles may produce local temperature increase. Second, the strong jet-flow pushed by an accelerating flame slows down at the obstacles and generates vortices in the pockets with high velocity gradients. Slowdown of the jet flow increases local pressure and temperature. Viscous dissipation of the vortices leads to additional

temperature increase, which has the same effect as viscous heating at the wall in smooth tubes [20, 34]. The important role of viscous heating in producing temperature peaks is especially obvious in Fig. 13 at the positions $Z/R = 25.75; 26; 26.25$, which are ahead of the strong shock position, $Z/R = 25.44$. At this simulation run explosion starts at an obstacle edge, as shown in Fig. 14. It is noted the exact position of explosion triggering may depend on the particular obstacle geometry, e.g. on the spacing between the obstacles. In Figs. 11, 14 we used a rather small spacing $\Delta z/R = 1/4$. Other simulations [12] performed for larger spacings also demonstrated the possibility of explosion triggering deep in the pockets with the hot spots produced by reflected shocks. Thus, both in Ref. [12] and in the present simulation, obstacles play an important role in explosion triggering and DDT.

5. SUMMARY

This paper presents the theory and numerical simulation of flame acceleration in channels with obstacles. We showed theoretically as well as computationally that flame acceleration is noticeably stronger in the axisymmetric geometry as compared to the planar one. We also considered the influence of gas compression on the flame acceleration, and showed numerically that the flame acceleration rate decreases with increasing initial Mach number, and that the velocity of the accelerating flame eventually saturates to a value that is supersonic with respect to the wall and is correlated to the known CJ deflagration speed. This saturation state has been referred to as that of fast flames in experimental studies [6, 21]. We also demonstrated numerically the possibility of DDT in the geometry of obstructed channels.

ACKNOWLEDGMENTS

This work was mostly supported by the Swedish Research Council (VR) and the Swedish Kempe Foundation. The numerical simulation was performed at the High Performance Computer Center North (HPC2N), Umea, Sweden, under SNAC project 007-07-25. The work at Princeton University was supported by the US Air Force Office of Scientific Research.

-
- [1] K. Shelkin, J. Exp. Teor. Phys. 10 (7) (1940) 823-827.
 - [2] Ya.B. Zeldovich, G.I. Barenblatt, V.B. Librovich, G.M. Makhviladze, Mathematical Theory of Combustion and Explosion, Consultants Bureau, New York, 1985.
 - [3] P.A. Urtiew, A.K. Oppenheim, Proc. R. Soc. Lond. A 295 (1966) 13-28.

- [4] J.E. Shepherd, J.H.S. Lee, Major Research Topics in Combustion, Springer-Verlag, Hampton, VA, 1992.
- [5] G.D. Roy, S.M. Frolov, A.A. Borisov, D.W. Netzer, Prog. Energy Combust. Sci. 30 (6) (2004) 545-672.
- [6] G. Ciccarelli, S. Dorofeev, Prog. En. Combust. Sci. 34 (4) (2008) 499-550.
- [7] G. Ciccarelli, C. Fowler, M. Bardon, Shock Waves 14 (3) (2005) 161-166.
- [8] M. Kuznetsov, V. Alekseev, I. Matsukov, S. Dorofeev, Shock Waves 14 (3) (2005) 205-215.
- [9] S. Frolov, I. Semenov, P. Utkin, P. Komissarov, V. Markov, Proceedings of 21st ICDERS, paper 215, Poitiers, France 2007.
- [10] C. Johansen, G. Ciccarelli, Proceedings of 21st ICDERS, paper 242, Poitiers, France 2007.
- [11] C. Johansen, G. Ciccarelli, Combust. Flame 156 (2) (2009) 405-416.
- [12] V. Gamezo, T. Ogawa, E. Oran, Proceedings of 21st ICDERS, paper 114, Poitiers, France 2007.
- [13] V. Gamezo, T. Ogawa, E. Oran, Combust. Flame 155 (1-2) (2008) 302-315.
- [14] V. Bychkov, A. Petchenko, V. Akkerman, L.E. Eriksson, Phys. Rev. E 72 (4) (2005) 046307.
- [15] V. Akkerman, V. Bychkov, A. Petchenko, L.E. Eriksson, Combust. Flame 145 (1-2) (2006) 206-219.
- [16] M. Wu, M. Burke, S. Son, R. Yetter, Proc. Combust. Inst. 31 (2) (2007) 2429-2436.
- [17] V. Bychkov, D. Valiev, L.E. Eriksson, Phys. Rev. Lett. 101 (16) (2008) 164501.
- [18] L.D. Landau, E.M. Lifshitz, Fluid Mechanics, Pergamon Press, Oxford, 1989.
- [19] R. Chue, J. Clarke, J.H. Lee, Proc. R. Soc. Lond. A 441 (1993) 607-623.
- [20] D. Valiev, V. Bychkov, V. Akkerman, L.E. Eriksson, Phys. Rev. E 80 (3) (2009) 036317.
- [21] M. Kuznetsov, V. Alekseev, Yu. Yankin, S. Dorofeev, Combust. Sci. Technol. 174 (5) (2002) 157-172.
- [22] C. Clanet, G. Searby, Combust. Flame 105 (1-2) (1996) 225-238.
- [23] V. Bychkov, V. Akkerman, G. Fru, A. Petchenko, (2) L.E. Eriksson, Combust. Flame 150 (4) (2007) 263-276.
- [24] V. Akkerman, V. Bychkov, A. Petchenko, L.E. Eriksson, Combust. Flame 145 (4) (2006) 675-687.
- [25] C.K. Law, Combustion Physics, Cambridge University Press, New York, NY, 2006.
- [26] L. Kagan, D. Valiev, M. Liberman, V. Gamezo, E. Oran, G. Sivashinsky, Effects Of Hydraulic Resistance And Heat Losses On The Deflagration-To-Detonation Transition, Pulse And Continuous Detonation Propulsion, Edited by G. Roy and S. Frolov, Torus Press, 2006, pp. 37-48.
- [27] O. Travnikov, M. Liberman, V. Bychkov, Phys. Fluids 9 (12) (1997) 3935-3937.
- [28] M. Modestov, V. Bychkov, D. Valiev, M. Marklund, Phys. Rev. E 80 (4) (2009) 046403.
- [29] N. Andersson, L.E. Eriksson, L. Davidsson, Int. J. Heat Fluid Flow 26 (3) (2005) 393-410.
- [30] N. Andersson, L.E. Eriksson, L. Davidsson, AIAA Journal 43 (9) (2005) 1899-1912.
- [31] C. Wollblad, L. Davidson, L.E. Eriksson, AIAA Journal 44 (10) (2006) 2340-2353.
- [32] V. Bychkov, M. Liberman, Phys. Reports 325 (4-5)(2000) 115-237.
- [33] V. Bychkov, V. Akkerman, Phys. Rev. E 73 (6) (2006) 066305.
- [34] D. Valiev, V. Bychkov, V. Akkerman, L.E. Eriksson, M. Marklund, Phys. Lett. A 372 (27-28)(2008) 4850-4857.
- [35] E. Oran, V. Gamezo, Combust. Flame 148 (1-2) (2007) 4-47.